

Saturation of the anomalous Hall effect at high magnetic fields in altermagnetic RuO₂

Teresa Tschirner,^{1,2} Philipp Keßler,^{2,3} Ruben Dario Gonzalez Betancourt,^{1,4} Tommy Kotte,⁵ Dominik Kriegner,^{4,6} Bernd Büchner,^{1,2,7} Joseph Dufouleur,¹ Martin Kamp,⁸ Vedran Jovic,⁹ Libor Smejkal,^{10,4} Jairo Sinova,^{10,4} Ralph Claessen,^{2,3} Tomas Jungwirth,^{4,11} Simon Moser,^{2,3} Helena Reichlova,^{4,6} and Louis Veyrat^{1,2,3}

¹*Leibniz Institute for Solid State and Materials Research, IFW Dresden, Helmholtzstr. 20, 01069 Dresden, Germany*

²*Würzburg-Dresden Cluster of Excellence ct.qmat, Germany*

³*Physikalisches Institut, Universität Würzburg, D-97074 Würzburg, Germany*

⁴*Institute of Physics ASCR, v.v.i., Cukrovarnická 10, 162 53, Prague, Czech Republic*

⁵*Hochfeld-Magnetlabor Dresden (HLD-EMFL), Helmholtz-Zentrum Dresden-Rossendorf, 01328 Dresden, Germany*

⁶*Institut für Festkörper- und Materialphysik, Technische Universität Dresden, 01069 Dresden, Germany*

⁷*Institute of Solid State and Materials Physics, TU Dresden, 01069 Dresden, Germany*

⁸*Physikalisches Institut, Universität Würzburg, D-97074 Würzburg, Germany; Röntgen Center for Complex Material Systems,*

Universität Würzburg, D-97074 Würzburg, Germany

⁹*Earth Resources and Materials, Institute of Geological and Nuclear Science, Lower Hutt 5010, New Zealand; MacDiarmid Institute for Advanced Materials and Nanotechnology, Wellington 6012, New Zealand;*

¹⁰*Institut für Physik, Johannes Gutenberg Universität Mainz, 55128 Mainz, Germany*

¹¹*School of Physics and Astronomy, University of Nottingham, NG7 2RD, Nottingham, United Kingdom*

(Dated: September 4, 2023)

Observations of the anomalous Hall effect in RuO₂ and MnTe have demonstrated unconventional time-reversal symmetry breaking in the electronic structure of a recently identified new class of compensated collinear magnets, dubbed altermagnets. While in MnTe the unconventional anomalous Hall signal accompanied by a vanishing magnetization is observable at remanence, the anomalous Hall effect in RuO₂ is excluded by symmetry for the Néel vector pointing along the zero-field [001] easy-axis. Guided by a symmetry analysis and ab initio calculations, a field-induced reorientation of the Néel vector from the easy-axis towards the [110] hard-axis was used to demonstrate the anomalous Hall signal in this altermagnet. We confirm the existence of an anomalous Hall effect in our RuO₂ thin-film samples whose set of magnetic and magneto-transport characteristics is consistent with the earlier report. By performing our measurements at extreme magnetic fields up to 68 T, we reach saturation of the anomalous Hall signal at a field $H_c \simeq 55$ T that was inaccessible in earlier studies, but is consistent with the expected Néel-vector reorientation field.

I. INTRODUCTION

The anomalous Hall effect (AHE) is a macroscopic linear response probe of time-reversal (\mathcal{T}) symmetry breaking in the electronic structure of magnetic materials [1–6]. The established mechanisms include \mathcal{T} -symmetry breaking and AHE in conventional ferromagnets or in non-collinear magnetic structures [1–9]. Recently, these have been extended by a novel and unconventional mechanism of \mathcal{T} -symmetry breaking resulting in prediction [2, 10] and subsequently observation of the AHE [11–13] in a class of compensated collinear magnets whose opposite magnetic moments reside on crystal-sublattices connected by rotation symmetries [2, 14, 15]. Materials of this third unconventional class of collinear magnets, complementing the conventional ferromagnetic and antiferromagnetic classes, have a characteristic alternating spin polarization in both real-space crystal structure and momentum-space electronic structure that suggests the term altermagnets [14, 15]. The \mathcal{T} -symmetry breaking nature of the AHE thus implies that the sign of the AHE in altermagnets flips when reversing the sign of the Néel vector [2, 10].

In contrast to ferromagnets, where AHE is always allowed, the AHE in altermagnets can be allowed or ex-

cluded by symmetry depending on the orientation of the Néel vector with respect to the crystal axes [2, 10]. (For a comprehensive symmetry discussion of AHE in ferromagnets, altermagnets and non-collinear magnets we refer to recent review articles in Refs. [1, 15]) In altermagnetic MnTe, for example, the AHE measured in the (0001) c -plane of this hexagonal crystal is allowed for the Néel vector pointing along one of the equivalent $(\bar{1}100)$ easy axes [11, 12]. As a result, Hall measurements in the (0001) c -plane show a hysteretic AHE signal of opposite sign at opposite saturating fields with a coercivity on the order of a few T when sweeping the magnetic field along the c -axis, with a finite remanent AHE at zero field.

Altermagnetic RuO₂ shows a qualitatively distinct AHE phenomenology [10, 11]. For the Néel vector along the magnetic easy-axis, which corresponds to the [001] axis of this tetragonal rutile crystal, the AHE is excluded by symmetry [2, 10]. An AHE is allowed by symmetry only when the Néel vector has a non-zero component in the (001) plane. As a result, no AHE signal is detected for a Hall bar patterned in the (001)-plane when sweeping the out-of-plane field along the [001] c -axis [11]. This sample and field geometry does not break the symmetry between opposite signs of the Néel-vector reorientation angle from the [001] easy axis [11, 16]. Therefore, even if

the applied field was strong enough to cause a spin-flop reorientation of the Néel vector towards the (001)-plane, it would not generate a non-zero net AHE signal odd in the applied field [11].

In contrast, a magnetic field applied along the [110] direction induces a continuous rotation of the Néel vector by an angle α from the [001] toward the [110] axis, given approximately by $\sin \alpha \sim H/H_c$ (for $H < H_c$) [11, 16]. Here, the direction of the Néel vector rotation is given by the sign of the magnetic field H , and H_c quantifies the field strength that aligns the Néel vector along the out-of-plane [110] axis. The critical field H_c hereby depends on the exchange interaction, the magneto-crystalline anisotropy, and the Dzyaloshinskii-Moriya interaction (DMI) terms of the thermodynamic potential [16] and in rutiles tends to be generally weaker than the spin-flop reorientation field applied along the [001] easy axis. In RuO_2 , H_c was estimated to be above 50 T, i.e. beyond the field available in the earlier AHE study [11], but below the [001] spin-flop field whose strength was estimated to exceed 100 T [11].

In the recent study [11], a non-linear Hall signal at high fields in RuO_2 Hall bars patterned in the (110)-plane was interpreted as a strong, yet unsaturated, AHE generated by the reorientation of the Néel vector into the (1 $\bar{1}$ 0)-plane by the applied [110] field. The opposite direction of the Néel vector rotation for opposite applied fields gave an opposite sign of the AHE [11]. The detected AHE signal was, therefore, odd in the applied [110]-field, and vanished at zero field. A comparison to the measurements in the (001)-plane Hall bars evidenced a strong AHE contribution in the (110)-plane samples, dominating the ordinary Hall contribution over the whole field range up to 50 T [11]. However, as H_c exceeded the experimentally available magnetic field range, no saturation of the AHE has been observed. The appearance of a saturation would make a strong case for an AHE generated by the Néel vector reorientation, for which such a saturation above H_c is expected.

In this study, we present magnetotransport measurements on (110)-plane oriented RuO_2 samples analogous to those explored in Ref. [11]. We further optimized the film preparation protocol to achieve high crystalline quality and stoichiometry, as evidenced by a thorough structural characterization. We performed on these samples a systematic magnetic and magneto-transport characterization up to magnetic fields of 68 T. Our results demonstrate consistency with Ref. [11] below 50 T, and by going beyond 50 T magnetic fields allows us to reach the saturation of the AHE signal. The observation of a saturation completes the experimental evidence of the AHE in this workhorse altermagnet [10, 11, 17–19].

II. THIN FILM GROWTH AND CHARACTERISATION

Our $\text{RuO}_2(110)$ samples were grown epitaxially on (110)-oriented substrates of rutile TiO_2 (CRYSTAL GmbH) using a commercial pulsed laser deposition (PLD) setup (TSST B.V.) with a pulsed excimer laser (COMPex Pro 205/KrF, 248 nm). Prior to growth, the substrates were cleaned in subsequent ultrasonic baths of isopropanol and acetone (20 min, puriss.) and annealed for 5 h in a tube furnace at 820 °C with an oxygen flow of 20 L/h to obtain a stepped-terrace morphology. The PLD growth conditions were set to an oxygen partial pressure of 1×10^{-3} mbar and a substrate temperature of 700 K (two-color pyrometer, IMPAC). Then, the sintered RuO_2 powder target (TOSHIMA manufacturing Co. Ltd.) was ablated by 32.000 laser pulses at a repetition rate of 10 Hz. The laser energy density was gradually increased from 0.7 to 1.4 J/cm² to compensate for laser induced oxygen deficiencies and a consequent increase of target reflectivity during deposition. The film growth was monitored by reflective high-energy electron diffraction (RHEED, STAIB) and post characterized by X-ray reflectivity (XRR) and X-ray diffraction (XRD) on a Rigaku Smartlab rotating anode with parabolic mirror and Ge channel cut monochromator using 8047.8 eV Cu $K\alpha$ radiation, as well as X-ray photoelectron spectroscopy (XPS, OMICRON, 1486.6 eV Al $K\alpha$; data not shown) to check the stoichiometry.

The film characterization results are shown in Fig. 1. Fig. 1a shows an XRD close-up around the 110 Bragg peak of the TiO_2 substrate and the epitaxial RuO_2 thin film, taken from the full range scan in the inset, and providing lattice parameters that are in excellent agreement with the literature values [11]. The data are further compared to simulations for a 9.8 nm thick film with 0.5 nm roughness, obtained via the Parrat formalism and a dynamic diffraction model as implemented in Ref. [20].

The XRR in Fig. 1b confirms the thickness of our sample to be $\approx 9 - 10$ nm. Both XRR and XRD show thickness fringes corresponding to the same thickness, proving excellent crystalline quality with a coherent crystal lattice from the interface with the substrate to the surface and correspondingly low roughness. The crystalline quality is further confirmed by transmission electron microscopy (TEM, FEI Titan 80-300, $U = 80-300$ kV, $I > 0.6$ nA) in Fig. 1d.

The low roughness suggested by XRD and XRR is consistently demonstrated by scanning tunneling microscopy (STM) images (Omicron VT-STM, constant current mode, RT, $U = 500$ mV, $I = 0.05$ nA) in Fig. 1c, yielding a rms of < 2 nm.

A superconducting quantum interference device (SQUID) MPMS3 magnetometry measurement of our sample at 5 K is shown in Fig. 1e. A measurement on a bare TiO_2 substrate is used as a reference to subtract the background from the data measured on the 9 nm RuO_2 film. As the signal from the magnetic RuO_2 moments

is extremely small as compared to the TiO_2 background, the presented magnetometry data is subject to a large error bar. However, the weak field-induced moment is consistent with the previous report by Feng et al. [11].

III. MAGNETO-TRANSPORT

To perform transport measurements, Hall bars were fabricated by e-beam lithography out of the RuO_2 thin films. Trenches defining the Hall bars were etched by argon ion beam etching. The Hall bars have different orientations in the sample (110) plane, either along the [001] or the $[\bar{1}\bar{1}1]$ axes, as shown in the inset of Fig. 2a. All Hall bars have a width of $10\ \mu\text{m}$, with distances between contacts of 50 and $100\ \mu\text{m}$, as shown in the second inset of Fig. 2a.

The magneto-transport measurements were first performed in static magnetic field in a standard Quantum Design Physical Properties Measurement System (QD PPMS) setup and afterwards the same device was studied in the high magnetic field laboratory (HLD) in Dresden-Rossendorf using pulsed magnetic fields up to 68 T, with pulses of 100 ms duration and a rise time of 35 ms. The magnetic field was applied in the out-of-plane sample direction, which corresponds to the RuO_2 [110] crystalline direction. To investigate the angular dependence of the Hall resistivity, the magnetic field was additionally tilted by $\theta = \pm 45^\circ$ towards [001], as illustrated in the inset of Fig. 4. An alternating current (AC) with an amplitude of $5\ \mu\text{A}$ was applied and the voltage was measured using a numerical lock-in technique with frequencies in the kHz range to suppress the noise level and spurious effects from the pulsed magnetic field. The presented high magnetic field data were measured on two samples grown under the same conditions showing reproducible results.

Fig. 2a shows the temperature dependent longitudinal resistivity ρ , which decreases with decreasing temperature, indicating metallic behavior in the thin films. The main result of our study is the Hall resistivity ρ_{Hall} measured up to 68 T, which is shown in Fig. 2b. The measurement in pulsed magnetic fields results in higher noise levels, therefore the curve was smoothed using a Savitzky-Golay filter and the noise is indicated by the error-bar. The Hall resistivity shows a pronounced non-linearity, exhibiting a non-zero curvature beyond 20 T. This is consistent with the measurements on $\text{RuO}_2(110)$ films reported in Ref. [11]. However, with the maximum accessible magnetic field of 50 T, a clear signature of the saturation of the AHE signal was not observed in Ref. [11]. In our data in Fig. 2b, we observe the saturation of the AHE above $H_c \simeq 55$ T. This field range is consistent with the expected 50 T-100 T scale of the reorientation field of the Néel vector from the [001] easy axis to the [110] hard axis [11]. Moreover, the very weak asymptotic slope above H_c (corresponding to the ordinary Hall effect), together with the overall magnitude of ρ_{Hall} , shows that the AHE signal dominates over the ordinary Hall

contribution over the entire range of applied magnetic fields.

Temperature-dependent magneto-transport data are shown in Fig. 3. The longitudinal magnetoresistance in Fig. 3a reaches 15% at 68 T and low temperature. At low fields, the magnetoresistance is roughly parabolic, and the amplitude of the magnetoresistance strongly decreases with increasing temperature. The temperature-dependent Hall resistivity is shown in Fig. 3b. The overall ρ_{Hall} amplitude decreases with increasing temperature, up to our maximum temperature of 200 K. In addition, we see a clear saturation of the Hall signal at temperatures up to 80 K.

Fig. 3c highlights the decrease in the Hall resistivity at 68 T with increasing temperature for two Hall bars patterned along the [001] and $[\bar{1}\bar{1}1]$ directions. The data of both samples are in remarkable agreement, indicating the Néel vector in both cases to be rotated into the (110) plane upon application of the [110] oriented magnetic field, as illustrated in the inset of Fig. 2a.

To further investigate the influence of a magnetic field component applied along the [001] easy axis on the AHE, we measure the Hall resistivity while tilting the field away from the [110] direction toward the [001] direction. The results are presented in Fig. 4, showing the Hall resistivity as a function of the [110] field component H_{\perp} for tilt angles of $\theta = \pm 45^\circ$. Again, all datasets are in remarkable agreement confirming that the AHE solely depends on the projection of the field onto the [110] axis. Most importantly, this implies that applying a magnetic field along the easy [001] axis does not tilt the Néel vector into the (110) plane, as this would result in saturation at lower fields.

IV. CONCLUSION

In conclusion, we have systematically investigated structural, magnetic and magneto-transport characteristics of epitaxial thin-film $\text{RuO}_2(110)$ grown on $\text{TiO}_2(110)$ substrates. The excellent crystalline quality of our films is demonstrated by XRR, TEM and STM measurements. Our magnetotransport results below 50 T are qualitatively consistent with the earlier report in Ref. [11] and provide an additional confirmation of the unconventional AHE originating from collinearly compensated magnetic order in altermagnetic RuO_2 .

Going beyond a mere confirmation, our work augments the range of accessible magnetic fields up to 68 T, fields that are large enough to saturate the AHE resistivity. The corresponding saturation field is consistent with earlier estimates [11].

Acknowledgements L.V. was supported by the Leibniz Association through the Leibniz Competition. Further funding support came from the Deutsche Forschungsgemeinschaft (DFG, German Research Foundation) under Germany's Excellence Strategy through the Würzburg-Dresden Cluster of Excellence on Com-

plexity and Topology in Quantum Matter ct.qmat (EXC 2147, Project ID 390858490) as well as through the Collaborative Research Center SFB 1170 ToCoTronics (Project ID 258499086). We further acknowledge fund-

ing support of the Czech Science Foundation Grant Nos. 19-18623X, GACR 22-17899K and DFG 490730630. Finally, this work was supported by HLD-HZDR, a member of the European Magnetic Field Laboratory (EMFL).

-
- [1] N. Nagaosa, J. Sinova, S. Onoda, A. H. MacDonald, and N. P. Ong, Anomalous Hall effect, *Reviews of Modern Physics* **82**, 1539 (2010), arXiv:0904.4154.
- [2] L. Šmejkal, A. H. MacDonald, J. Sinova, S. Nakatsuji, and T. Jungwirth, Anomalous Hall antiferromagnets, *Nature Reviews Materials* **7**, 482 (2022), arXiv:2107.03321.
- [3] R. Shindou and N. Nagaosa, Orbital Ferromagnetism and Anomalous Hall Effect in Antiferromagnets on the Distorted fcc Lattice, *Physical Review Letters* **87**, 116801 (2001), arXiv:0108322 [cond-mat].
- [4] Y. Machida, S. Nakatsuji, S. Onoda, T. Tayama, and T. Sakakibara, Time-reversal symmetry breaking and spontaneous Hall effect without magnetic dipole order, *Nature* **463**, 210 (2010).
- [5] H. Chen, Q. Niu, and A. H. Macdonald, Anomalous hall effect arising from noncollinear antiferromagnetism, *Physical Review Letters* **112**, 017205 (2014), arXiv:1309.4041.
- [6] J. Kübler and C. Felser, Non-collinear antiferromagnets and the anomalous Hall effect, *Epl* **108**, 67001 (2014), arXiv:1410.5985.
- [7] S. Nakatsuji, N. Kiyohara, and T. Higo, Large anomalous Hall effect in a non-collinear antiferromagnet at room temperature, *Nature* **527**, 212 (2015).
- [8] N. Kiyohara, T. Tomita, and S. Nakatsuji, Giant anomalous hall effect in the chiral antiferromagnet mn_3Ge , *Phys. Rev. Appl.* **5**, 064009 (2016).
- [9] A. K. Nayak, J. E. Fischer, Y. Sun, B. Yan, J. Karel, A. C. Komarek, C. Shekhar, N. Kumar, W. Schnelle, J. Kübler, C. Felser, and S. S. Parkin, Large anomalous Hall effect driven by a nonvanishing Berry curvature in the noncolinear antiferromagnet Mn_3Ge , *Science Advances* **2**, e1501870 (2016), arXiv:1511.03128.
- [10] L. Šmejkal, R. González-Hernández, T. Jungwirth, and J. Sinova, Crystal time-reversal symmetry breaking and spontaneous Hall effect in collinear antiferromagnets, *Science Advances* **6**, eaaz8809 (2020), arXiv:1901.00445.
- [11] Z. Feng, X. Zhou, L. Šmejkal, L. Wu, Z. Zhu, H. Guo, R. González-Hernández, X. Wang, H. Yan, P. Qin, X. Zhang, H. Wu, H. Chen, Z. Meng, L. Liu, Z. Xia, J. Sinova, T. Jungwirth, and Z. Liu, An anomalous Hall effect in altermagnetic ruthenium dioxide, *Nature Electronics* **5**, 735 (2022).
- [12] R. D. Gonzalez Betancourt, J. Zubáč, R. Gonzalez-Hernandez, K. Geishendorf, Z. Šobáň, G. Springholz, K. Olejník, L. Šmejkal, J. Sinova, T. Jungwirth, S. T. B. Goennenwein, A. Thomas, H. Reichlová, J. Železný, and D. Kriegner, Spontaneous Anomalous Hall Effect Arising from an Unconventional Compensated Magnetic Phase in a Semiconductor, *Physical Review Letters* **130**, 036702 (2023), arXiv:2112.06805.
- [13] K. Samanta, M. Ležaić, M. Merte, F. Freimuth, S. Blügel, and Y. Mokrousov, Crystal Hall and crystal magneto-optical effect in thin films of SrRuO_3 , *Journal of Applied Physics* **127**, 213904 (2020).
- [14] L. Šmejkal, J. Sinova, and T. Jungwirth, Beyond Conventional Ferromagnetism and Antiferromagnetism: A Phase with Nonrelativistic Spin and Crystal Rotation Symmetry, *Physical Review X* **12**, 031042 (2022).
- [15] L. Šmejkal, J. Sinova, and T. Jungwirth, Emerging Research Landscape of Altermagnetism, *Physical Review X* **12**, 040501 (2022), arXiv:2204.10844.
- [16] A. N. Bazhan and C. Bazan, Weak ferromagnetism in CoF_2 and NiF_2 , *Sov Phys JETP* **42**, 898 (1976).
- [17] A. Bose, N. J. Schreiber, R. Jain, D.-f. Shao, H. P. Nair, J. Sun, X. S. Zhang, D. A. Muller, E. Y. Tsymbal, D. G. Schlom, and D. C. Ralph, Tilted spin current generated by an antiferromagnet, *Nature Electronics* **5**, 263 (2022), arXiv:2108.09150.
- [18] H. Bai, L. Han, X. Y. Feng, Y. J. Zhou, R. X. Su, Q. Wang, L. Y. Liao, W. X. Zhu, X. Z. Chen, F. Pan, X. L. Fan, and C. Song, Observation of Spin Splitting Torque in a Collinear Antiferromagnet RuO_2 , *Physical Review Letters* **128**, 197202 (2022), arXiv:2109.05933.
- [19] S. Karube, T. Tanaka, D. Sugawara, N. Kadoguchi, M. Kohda, and J. Nitta, Observation of Spin-Splitter Torque in Collinear Antiferromagnetic RuO_2 , *Physical Review Letters* **129**, 137201 (2022), arXiv:2111.07487.
- [20] D. Kriegner, E. Wintersberger, and J. Stangl, *xrayutilities*: a versatile tool for reciprocal space conversion of scattering data recorded with linear and area detectors, *Journal of Applied Crystallography* **46**, 1162 (2013).

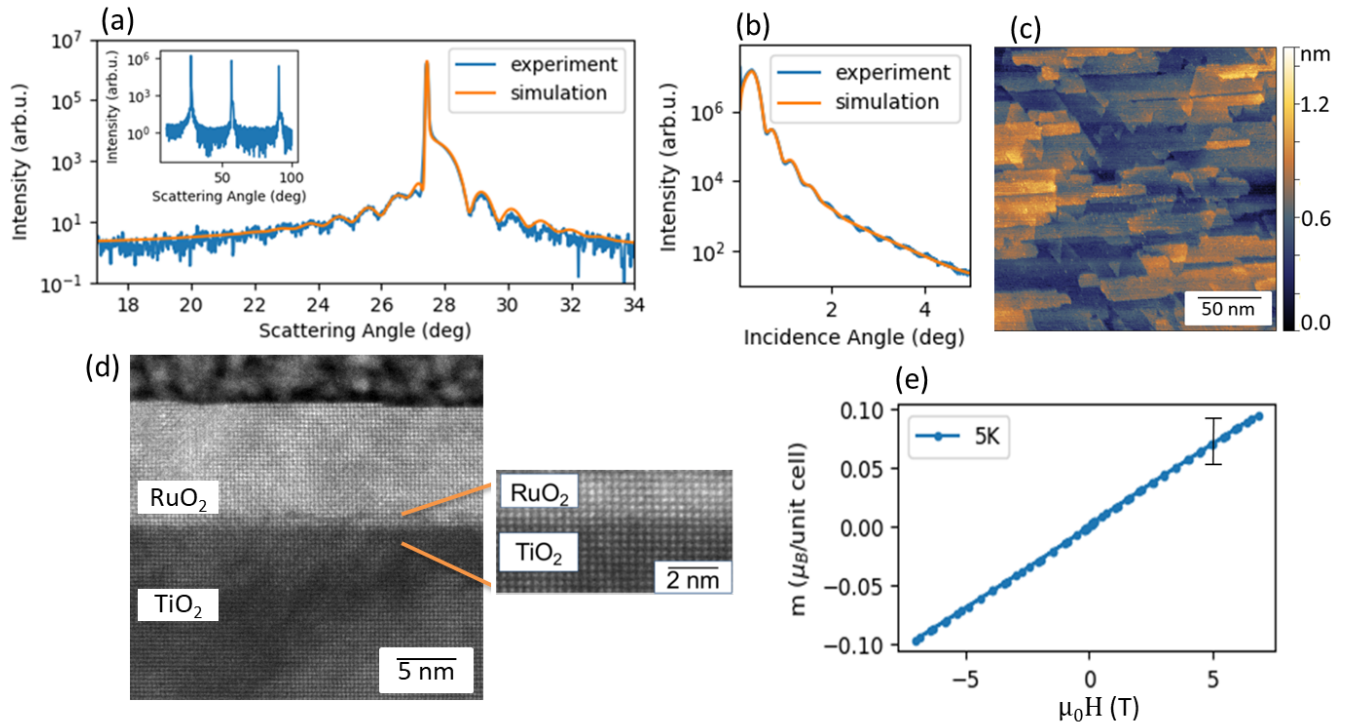


FIG. 1. **Growth and characterisation of RuO₂ thin film on a TiO₂(110).**(a) XRD data of the 110 Bragg peak (full range in the inset) and (b) XRR show good agreement with simulations for a 9.8 nm thick film with 0.5 nm roughness. (c) STM shows a smooth film surface. (d) TEM shows epitaxial and dislocation-free growth of RuO₂(110) on TiO₂(110). (e) SQUID magnetometry measurements on the RuO₂/TiO₂ sample with subtracted background based on a TiO₂ reference measurement. The large error bar of the magnetization data is due to the weak field-induced magnetic moments in RuO₂

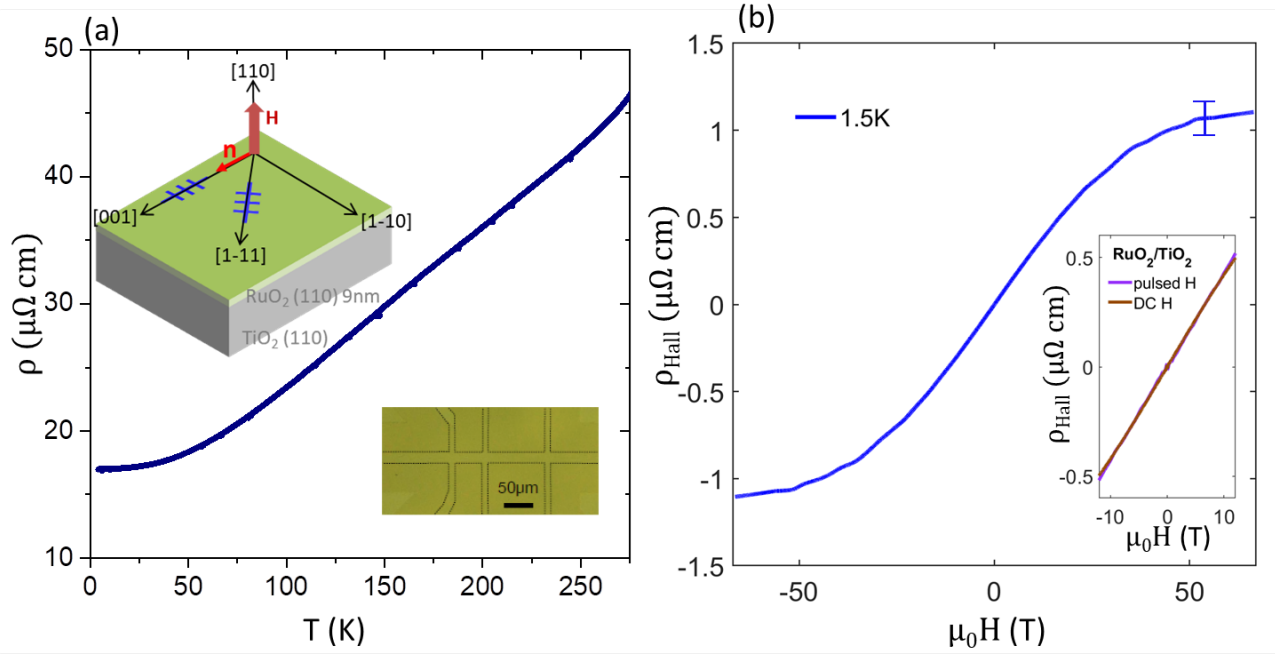


FIG. 2. **Magneto-transport in (110)-oriented RuO_2 thin films.** (a) Temperature dependence of the longitudinal resistivity showing metallic behavior. Upper inset: Orientation of the Hall bars with respect to the crystal directions and the directions of the Néel-vector easy axis (\mathbf{n}) and applied field axis (\mathbf{H}). Lower inset: optical microscopy image of the RuO_2 Hall bar, highlighted by dashed lines. (b) Antisymmetrized transverse resistivity (Hall resistivity) of a RuO_2 Hall bar oriented in the [001] direction measured in the high magnetic field facility up to 68 T. The inset compares the pulsed field to the in house static field measurements up to 12 T.

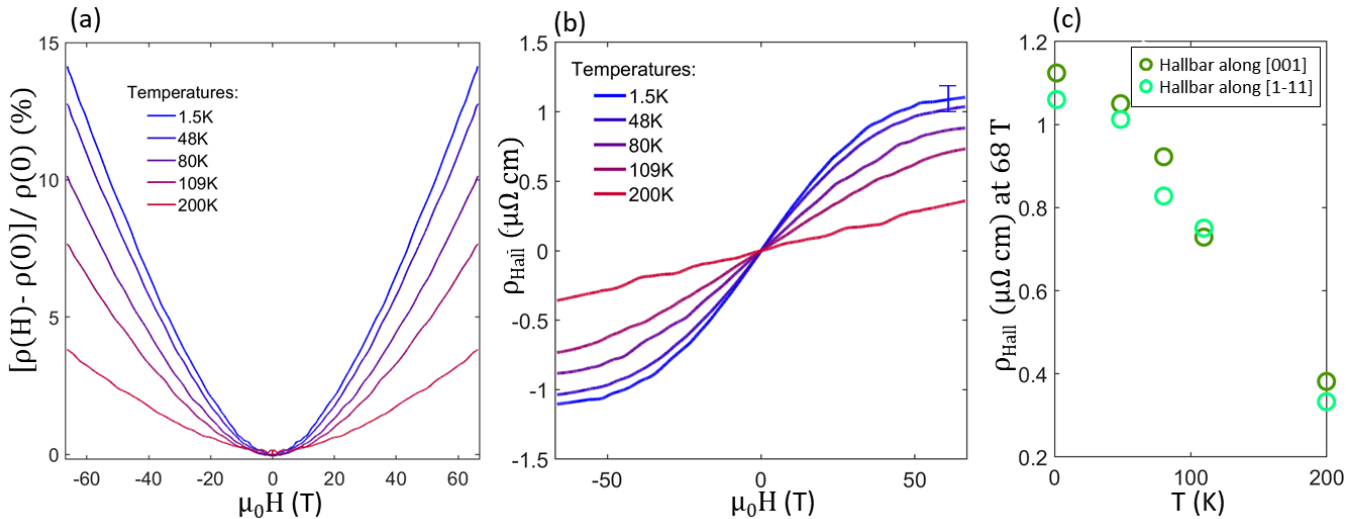


FIG. 3. **Temperature dependent magneto-transport data of $\text{RuO}_2(110)$.** (a) Temperature dependence of the symmetrized longitudinal magnetoresistance and (b) the antisymmetrized transverse resistivity (Hall resistivity). The error-bar indicates the uncertainties caused by noise in high magnetic fields. (c) Comparison of the temperature dependencies of the Hall resistivity at $B=68$ T for Hall bars oriented along the [001] and [111] directions, respectively.

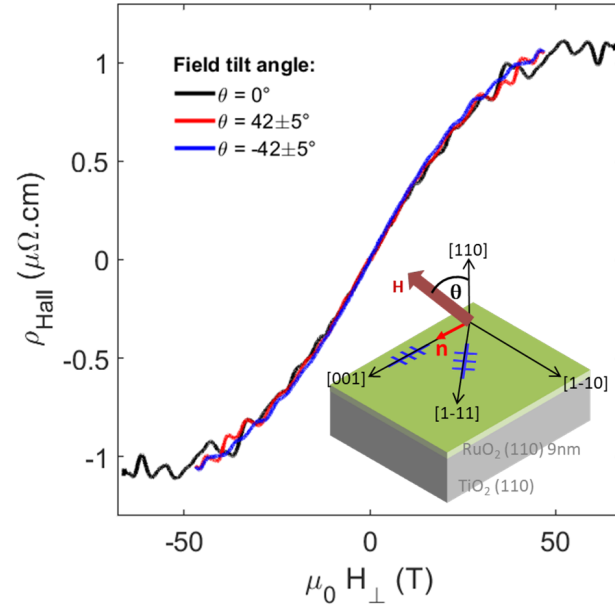


FIG. 4. **Effect of magnetic field tilting on the Hall resistivity in $\text{RuO}_2(110)$.** The Hall resistivity is shown with respect to the out-of-plane component of the tilted magnetic field. The magnetic field was rotated by $\pm 45^\circ$ toward the $[001]$ axis. The inset shows the orientation of the Hall bars with respect to the crystal directions of the Néel-vector easy axis (\mathbf{n}) and the applied field axis (\mathbf{H}) rotated at an angle θ .